

Article

Phase Behavior and Defect Structure of $\text{HoBaCo}_2\text{O}_{6-\delta}$

Roman E. Yagovitin ^{*}, Dmitry S. Tsvetkov ^{*}, Ivan L. Ivanov , Dmitry A. Malyshkin, Vladimir V. Sereda 
and Andrey Yu. Zuev 

Institute of Natural Sciences and Mathematics, Ural Federal University, 19 Mira St., 620002 Ekaterinburg, Russia; ivan.ivanov@urfu.ru (I.L.I.); dmitry.malyshkin@urfu.ru (D.A.M.); vladimir.sereda@urfu.ru (V.V.S.); andrey.zuev@urfu.ru (A.Y.Z.)

^{*} Correspondence: roman.iagovitin@urfu.ru (R.E.Y.); dmitry.tsvetkov@urfu.ru (D.S.T.)

Abstract: The differential scanning calorimetry study showed that the double perovskite $\text{HoBaCo}_2\text{O}_{6-\delta}$ (HBC), depending on its oxygen content, undergoes three phase transitions in the temperature range 298–773 K. Their origin was tentatively explained using the relevant literature data. For the single-phase tetragonal HBC, the oxygen nonstoichiometry dependences on the oxygen partial pressure were investigated by thermogravimetric and flow reactor methods in the intermediate-temperature range of 573–773 K. The proposed defect structure of HBC was successfully verified using the obtained data on its oxygen nonstoichiometry combined with those reported earlier. As a result, the values of the thermodynamic parameters (ΔH_i° , ΔS_i°) of the defect reactions proceeding in HBC were determined. The defect structure of HBC was shown to be similar to that of $\text{YBaCo}_2\text{O}_{6-\delta}$ (YBC) likely due to similar ionic radii of Ho^{3+} and Y^{3+} .

Keywords: phase transitions; point defects; defect equilibria; nonstoichiometry



Citation: Yagovitin, R.E.; Tsvetkov, D.S.; Ivanov, I.L.; Malyshkin, D.A.; Sereda, V.V.; Zuev, A.Y. Phase Behavior and Defect Structure of $\text{HoBaCo}_2\text{O}_{6-\delta}$. *Inorganics* **2023**, *11*, 361. <https://doi.org/10.3390/inorganics11090361>

Academic Editor: Richard Dronskowski

Received: 23 July 2023

Revised: 24 August 2023

Accepted: 28 August 2023

Published: 5 September 2023



Copyright: © 2023 by the authors. Licensee MDPI, Basel, Switzerland. This article is an open access article distributed under the terms and conditions of the Creative Commons Attribution (CC BY) license (<https://creativecommons.org/licenses/by/4.0/>).

1. Introduction

Double perovskites with formula $\text{REBaCo}_2\text{O}_{6-\delta}$, where RE is a rare-earth metal, have a set of unique properties, such as high total and oxide ion conductivity and rapid oxygen exchange with ambient atmosphere [1–4]. That is why these oxides are regarded as extremely promising for a variety of energy conversion applications, from solid oxide fuel cells (SOFCs) [1–8], including those with proton-conducting electrolytes [9], to oxygen-permeating dense ceramic membranes [10,11], data storage of magnetic devices [12,13] and catalysts [14,15]. Nowadays the double perovskites containing relatively large early rare-earth elements (from La to Gd) were studied more extensively [16–25], whilst those containing smaller rare-earth elements were investigated relatively poorly. At the same time, it is the double perovskites with rare-earth elements of smaller size such as Y and Ho that possess modest value of thermal expansion coefficient ($\sim 15 \cdot 10^{-6} \text{ K}^{-1}$ at $T = 773\text{--}1173 \text{ K}$ [26]) attractive for SOFCs' cathode applications. This warrants more thorough investigation of the fundamental properties, including the phase composition, phase behavior, crystal structure, and oxygen content, of these oxides as the target materials for further modifications.

Oxygen nonstoichiometry was shown to affect various properties of $\text{REBaCo}_2\text{O}_{6-\delta}$, including magnetic properties [27], temperatures of phase transitions and thermodynamic properties [27,28], and electronic and oxide ion transport [29]. It is of great importance to highlight that the oxygen content of an oxide material, being measured reliably depending on temperature (T) and oxygen partial pressure ($p\text{O}_2$), enables validating its defect structure model and, consequently, evaluating the thermodynamics of defect interactions. At the same time, an adequate defect structure model is of key importance for describing and controlling many, if not most, target properties of nonstoichiometric oxides as materials for a variety of applications, including energy storage and conversion [29,30].

Double perovskites $\text{REBaCo}_2\text{O}_{6-\delta}$ possess either tetragonal (space group $P4/mmm$) or orthorhombic structure (space group $Pmmm$) depending on oxygen content and temperature. Also, upon variation of the size of the RE^{3+} -cation and nature of the dopants in the Ba-

and Co-sublattices transition to ‘simple’ cubic perovskite structure (space group $Pm-3m$) is possible under certain conditions (temperature and oxygen partial pressure) [31].

The Y-containing double perovskite cobaltite, YBC, was shown [28] to undergo two structural transitions upon increasing temperature: the first tetragonal ($P4/mmm$, 332-type superstructure) phase transforms to an orthorhombic ($Pmmm$ and 122-type superstructure) one and then to a tetragonal phase ($P4/mmm$, 112-type superstructure). The former transition occurs due to the change of the ordering pattern of oxygen vacancies and the latter because of complete disordering of oxygen vacancies.

HoBaCo₂O_{5.3}, in turn, was shown to possess a tetragonal structure (space group $P4/mmm$, 112-type superstructure) as a result of holmium and barium atoms ordering along the c -axis [16]. Formation of superstructure with tripled parameters a and b (space group $P4/mmm$, 332-type superstructure) as a result of oxygen vacancies ordering was reported in [16,32]. However, it was not observed in [27]. Therefore, the fine crystal structure of HBC, including different superstructures, remains a controversial topic.

Oxygen nonstoichiometry of REBaCo₂O_{6- δ} was studied for the oxides containing the following rare-earth elements: La [33], Pr [29], Nd [34], Sm [35], Eu [35], and Gd [36]. Several methods were employed in the previous works to measure the oxygen nonstoichiometry of YBC: coulometric titration at high temperatures, 1173–1323 K [37], and thermogravimetry and flow reactor method at moderate temperatures, 573–773 K [28]. The results of the latter were used to make the proposed defect structure model [38] applicable not only in the relatively narrow range of high temperatures (1173–1323 K), but also at lower temperatures, down to 573 K. It was found that the re-evaluated enthalpies and entropies of defect interactions in YBC are close to those for GdBaCo₂O_{6- δ} , being distinctively different from those for the other REBaCo₂O_{6- δ} with larger rare-earth ions [28]. Unlike YBC, the oxygen nonstoichiometry of HBC was only measured either in a narrow high-temperature range of 1173 to 1323 K at pO_2 between 1 and 10^{-5} atm [37], or in a wider temperature range but at pO_2 lower than 10^{-4} atm [27]. The oxygen content of HBC, $6-\delta$, was shown to change under studied conditions in narrow span from 5.02 to 4.98 [37]. It is worth mentioning that a defect structure model evaluated in [37] does not describe the data presented in [27]. Therefore, one can conclude that the oxygen content of HBC needs to be measured reliably in the extended ranges of T and pO_2 and its defect structure remains poorly defined.

It should be noticed that HBC, as with YBC [38,39], has a limited thermodynamic stability range. It decomposes into BaCoO_{3- δ} and HoCoO_{3- δ} at 1073 K in air atmosphere [40] and becomes stable only at temperatures higher than 1173 K [37]. However, at temperatures lower than 1073 K, HBC is stable because of kinetic factor [37,40]. Therefore, oxygen nonstoichiometry in HBC may be measured reversibly not only at temperatures higher than 1173 K, as it has been conducted in [37], but also at temperatures lower than 1073 K, as in YBC. It is of great interest to model the defect structure of HBC in the extended temperature range and compare modeling results with those for defect structure of other double perovskites studied earlier. Besides, since HBC is regarded, as with other REBaCo₂O_{6- δ} oxides, as a promising material for applications at intermediate temperatures, its phase behavior should be studied at temperatures lower than 1073 K.

Thereby, this study was aimed at: (i) elucidation of the phase behavior of HBC between room temperature and 773 K; (ii) obtaining experimental pO_2 - T - δ data for this oxide at the low and intermediate temperatures, 573–773 K, using the thermogravimetric and flow reactor methods, suitable for the measurements in these conditions; and (iii) describing the defect chemistry of HBC and thermodynamics of its disordering in the extended temperature range, 573–1323 K.

2. Experimental

The powder sample of HoBaCo₂O_{6- δ} was synthesized using the standard ceramic technique using Ho₂O₃, BaCO₃, and Co₃O₄ as the precursors. The details of the synthesis procedure were described elsewhere [28]. After the final annealing step at 1373 K for 24 h, to avoid the decomposition of the sample, it was rapidly cooled to 773 K in air, held for 5 h

in these conditions, and then cooled to room temperature with a $100 \text{ K}\cdot\text{h}^{-1}$ cooling rate. X-ray diffraction (XRD) was used to confirm the phase purity of the synthesized sample. The XRD pattern was obtained using an XRD-7000 diffractometer (Shimadzu, Kyoto, Japan) with $\text{Cu K}\alpha$ radiation. Indexing and Rietveld refinement of the XRD patterns were carried out using the Rietica software package [41].

The chemical composition and morphology of the as-prepared powder sample was examined using a VEGA 3 scanning electron microscope (Tescan, Brno, Czech Republic) equipped with an Ultim Max 40 detector (Oxford Instruments, Abingdon, UK).

Thermogravimetric (TG) measurements were performed with a DynTherm LP-ST (Rubotherm, Bochum, Germany) thermobalance. The absolute oxygen nonstoichiometry in the $\text{HoBaCo}_2\text{O}_{6-\delta}$ was determined by the direct reduction in a flow of H_2/N_2 gas mixture (1:1 by volume, $100 \text{ mL}\cdot\text{min}^{-1}$ total gas flow) at 1323 K in the thermobalance. The experimental techniques are described in detail elsewhere [42]. The oxygen content, $(6-\delta)$, in the $\text{HoBaCo}_2\text{O}_{6-\delta}$ sample slowly ($100 \text{ K}\cdot\text{h}^{-1}$) cooled in air was found to be 5.350 ± 0.005 .

Oxygen nonstoichiometry in $\text{HoBaCo}_2\text{O}_{6-\delta}$ was also independently measured by the flow reactor method. The original experimental setup used for the flow reactor measurements and step-by-step relaxation procedure were described in detail elsewhere [28].

The MHTC 96 (Setaram, Caluire, France) calorimeter equipped with a differential scanning calorimetry (DSC) sensor was employed for investigating the phase behavior of $\text{HoBaCo}_2\text{O}_{6-\delta}$ in different atmospheres. The atmosphere around the sample was controlled by sweeping the calorimetric cell with mixtures of dry air and dry N_2 ($p_{\text{O}_2} = 10^{-4.3}$ atm), prepared using RRG-12 (Eltochpribor, Zelenograd, Russia) mass-flow controllers. The exact oxygen content (p_{O_2}) in the sweeping gas was measured at the outlet of the calorimeter by an external potentiometric YSZ oxygen sensor. The total gas flow rate was $100 \text{ mL}\cdot\text{min}^{-1}$. The combined thermal and caloric calibration of the DSC setup was carried out using the heats and temperatures of fusion of high-purity standard metals (Ga, In, Sn, Pb, Al).

Because the stability issues and the phase behavior were expected to be quite similar for two double perovskites $\text{RBaCo}_2\text{O}_{6-\delta}$ ($\text{R} = \text{Ho}, \text{Y}$), for the DSC measurements performed for $\text{HoBaCo}_2\text{O}_{6-\delta}$ in the present work we followed the same procedure as was used for $\text{YBaCo}_2\text{O}_{6-\delta}$ in our previous study [28]. This also facilitates a direct comparison between the DSC curves obtained for these two oxides.

3. Results and Discussion

3.1. Sample Characterization and Phase Behavior

The XRD pattern of the as-prepared sample of $\text{HoBaCo}_2\text{O}_{5.35}$ is shown in Figure 1. It was indexed using $P4/mmm$ space group employed earlier for $\text{YBaCo}_2\text{O}_{5.33}$ [28]. The results of the Le Bail fitting ($\chi^2 = 1.4$) are also shown in Figure 1. The refined lattice constants, $a = b = 11.629(1) \text{ \AA}$ and $c = 7.498(1) \text{ \AA}$, were found to be in good agreement with ones reported previously [16,37].

The SEM-EDX micrographs of the $\text{HoBaCo}_2\text{O}_{5.35}$ sample are shown in Figure 2. As seen, the powder possesses micron-size particles with uniform distribution of elements. The measured and nominal compositions of the sample were found to be in good agreement with each other.

The results of the DSC studies of the phase behavior of HBC in the atmospheres with different p_{O_2} are given in Figures 3 and 4. Figure 3 indicates that the number of phase transitions and the shape of the DSC curves strongly depend on the oxygen content in the sample as evidenced, for example, by the comparison of the curves recorded at $\log(p_{\text{O}_2}/\text{atm}) = -0.68, -1.0$ and -1.5 . As seen, even the change of the oxygen content as small as 0.02 significantly affects the shape of the DSC curve. As a result, depending on the oxygen content, $6-\delta$, HBC exhibits 1 to 3 phase transitions at temperatures T_1, T_2 , and T_3 , respectively, upon heating in the range of 298 to 573 K. At higher temperatures, the onset of the large endothermic peak is obviously seen on the DSC curves recorded for all HBC samples except that with the lowest oxygen content (5.00). This peak corresponds to oxygen release from HBC lattice.

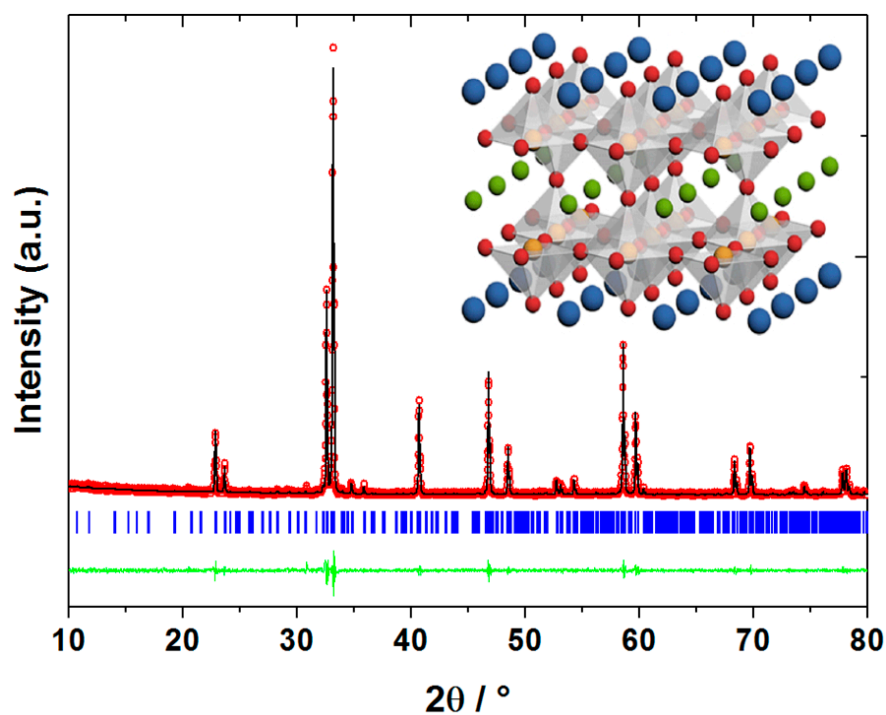


Figure 1. Refined XRD pattern of $\text{HoBaCo}_2\text{O}_{5.35}$; red points—experimental data, black line—calculated pattern, green line—difference between the experimental and calculated data, blue ticks—positions of the allowed Bragg reflections. Inset shows schematically the double perovskite structure; blue, green, orange and red spheres correspond to barium, holmium, cobalt and oxygen atoms respectively.

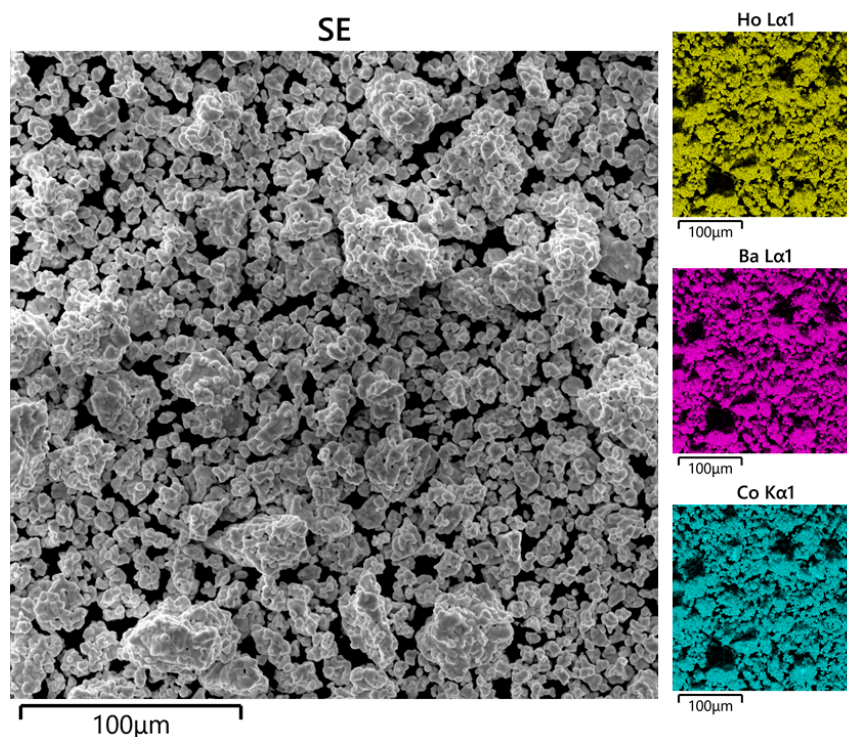


Figure 2. Results of the morphology and chemical composition study for $\text{HoBaCo}_2\text{O}_{5.35}$ powder sample: (left) electron image in the secondary electrons (SE) mode; (right) element distribution maps (energy-dispersive X-ray (EDX) spectroscopy): Ho; Ba; Co.

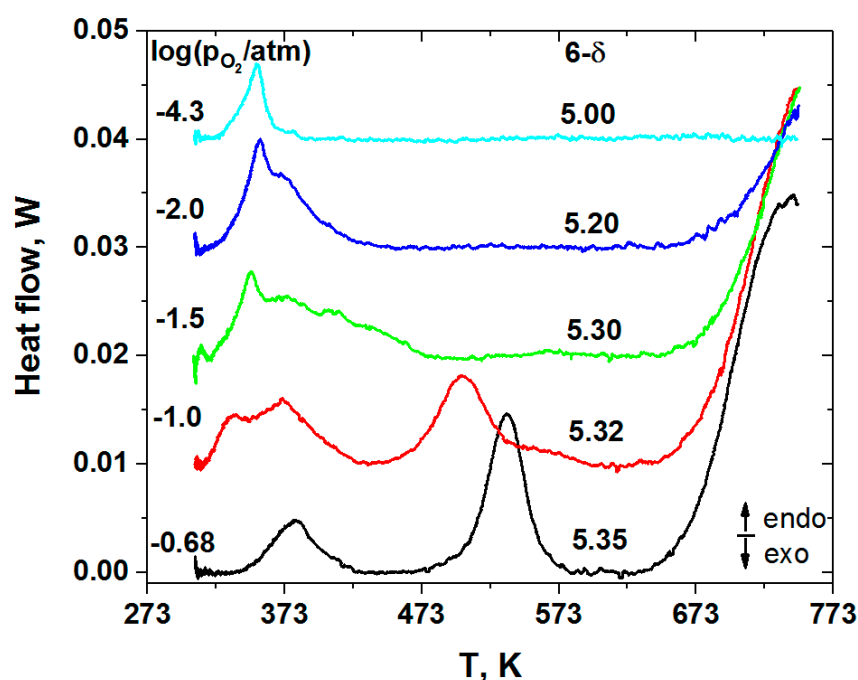


Figure 3. The DSC curves recorded at different p_{O_2} for the $\text{HoBaCo}_2\text{O}_{6-\delta}$ samples with different initial oxygen nonstoichiometry. For the sake of convenience, the curves are shifted relative to each other.

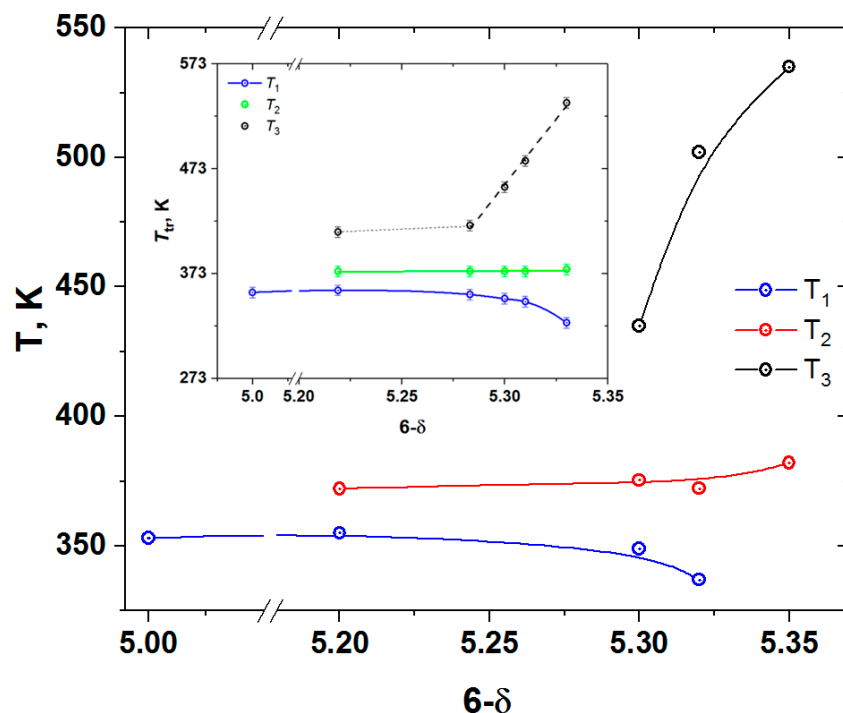


Figure 4. The dependences of the phase transition temperatures in $\text{HoBaCo}_2\text{O}_{6-\delta}$ on its oxygen content. The inset shows similar transition temperatures in $\text{YBaCo}_2\text{O}_{6-\delta}$ [28].

Figure 4 shows that the transition temperatures (determined as maxima of the corresponding DSC-peaks) depend to some extent on the oxygen content in HBC. As seen, T_3 increases strongly with oxygen content whereas its variation induces only small changes at T_1 and T_2 . Similar phase behavior was found earlier for YBC [28]. For the sake of comparison, variation of the phase transition temperatures with oxygen content in YBC is shown in the inset of Figure 4.

Such similarity in the observed phase behavior of the double perovskites containing Ho and Y can be explained by the almost equal radii of these cations [43]. This allows us to interpret the origin of the phase transitions in HBC in the same way as in the Y-containing analog. The transition observed at the lowest temperature, T_1 , is, most probably, of magnetic origin [28]. Suard and Fauth also found magnetic phase transition for $\text{HoBaCo}_2\text{O}_5$ at $T = 340 \text{ K}$ [44,45] i.e., close to temperature of phase transition detected in the present work. The middle-temperature phase transition, occurring at T_2 , may be identified with the transition of the tetragonal phase with s.g. $P4/mmm$ and 332-type superstructure to the orthorhombic phase with s.g. $Pmmm$ and 122-type superstructure, associated with the change in the ordering pattern of oxygen vacancies [28]. Finally, the phase transition at the high temperature, T_3 , seems to be the result of complete disordering of oxygen vacancies and formation of tetragonal phase, which is characterized by s.g. $P4/mmm$ and 112-superstructure [28]. Thus, at temperatures higher than 573 K, HBC possesses $P4/mmm$ tetragonal crystal structure and all the results of the oxygen content determination and defect structure analysis presented and discussed further correspond to this particular phase state of HBC.

3.2. Oxygen Nonstoichiometry and Defect Structure of $\text{HoBaCo}_2\text{O}_{6-\delta}$

In previous studies, the oxygen nonstoichiometry of HBC was measured only in the high-temperature range of 1173 to 1373 K [37]. At temperatures lower than 1123 K, this oxide is thermodynamically metastable in air [40]. However, the XRD pattern of the HBC sample annealed at 773 K for 100 h did not reveal any evidence of HBC decomposition [40]. This means that below 773 K, a rate of the solid-state reaction of HBC decomposition becomes so low that this oxide can be regarded as kinetically stable. For this reason, the temperature of 773 K was selected as the upper limit of the temperature range, in which the oxygen nonstoichiometry, δ , of $\text{HoBaCo}_2\text{O}_{6-\delta}$ was measured in the present work. In turn, at a temperature as low as 573 K, HBC still exhibits relatively fast oxygen exchange with the ambient atmosphere, simultaneously retaining, as mentioned above, the same tetragonal crystal structure.

Figure 5 shows the experimental data on the oxygen nonstoichiometry, δ , in $\text{HoBaCo}_2\text{O}_{6-\delta}$, measured using different techniques as a function of T and $p\text{O}_2$. The results of high temperature coulometric titration measurements reported in [37] are also given in Figure 5 for comparison. As seen in Figure 5, the results obtained by TG and flow reactor methods are in good agreement with each other. Furthermore, oxygen nonstoichiometry at lower temperatures varies in the wide range from 0.600 to 0.929, whereas at high temperatures it is close to 1 and changes with $p\text{O}_2$ only slightly. Similar observations were also reported earlier for YBC [28]. It is worth mentioning that the oxygen content in $\text{HoBaCo}_2\text{O}_{6-\delta}$ and $\text{YBaCo}_2\text{O}_{6-\delta}$ is about the same as shown in Figure 6, where that is given as a function of temperature in air for both double perovskites.

The combined dataset shown in Figure 5, including both the oxygen nonstoichiometry measured in the present work and that reported elsewhere [37], was used for verification of the HBC defect structure model reported by us in an earlier study [28,29,34–36]. The defect reactions considered within the framework of this model are shown in Table 1.

Table 1. The defect structure analysis results for $\text{HoBaCo}_2\text{O}_{6-\delta}$.

No.	Reaction	$\Delta S_i^\circ, \frac{\text{J}}{\text{mol}\cdot\text{K}}$	$\Delta H_i^\circ, \frac{\text{kJ}}{\text{mol}}$	R^2
1	$2\text{Co}_{\text{Co}}^\times \rightleftharpoons \text{Co}'_{\text{Co}} + \text{Co}_{\text{Co}}$	0 ^b	21.6 ± 3.0 ^a	0.985
2	$\text{Ho}_{\text{Ho}}^\times + \text{V}_{\text{O}}^\bullet \rightleftharpoons (\text{Ho}_{\text{Ho}}^\times \text{V}_{\text{O}}^\bullet)^{\bullet\bullet}$	0 ^b	-115.8 ± 1.3 ^a	
3	$2\text{Co}_{\text{Co}}^\times + \text{O}_{\text{O}}^\times + \text{Ho}_{\text{Ho}}^\times \rightleftharpoons \frac{1}{2}\text{O}_{2(\text{g})} + (\text{Ho}_{\text{Ho}}^\times \text{V}_{\text{O}}^\bullet)^{\bullet\bullet} + 2\text{Co}'_{\text{Co}}$	70.2 ± 1.5 ^a	66.5 ± 1.5 ^a	

^a The values following the «±» symbol correspond to expanded standard uncertainty calculated based on the Levenberg–Marquardt fitting procedure at the level of confidence $\approx 95\%$. ^b The value was fixed as 0 during the fitting procedure [28,29,34–36].

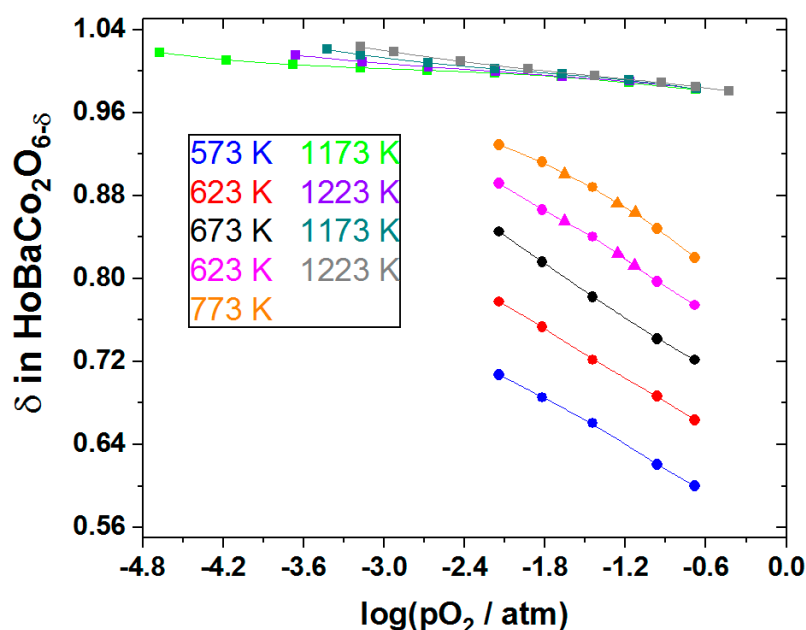


Figure 5. Oxygen nonstoichiometry in $\text{HoBaCo}_2\text{O}_{6-\delta}$ as function of T and $p\text{O}_2$; ●—data obtained by thermogravimetric analysis, ▲—data obtained by flow reactor method, ■—data obtained by coulometric titration in [37].

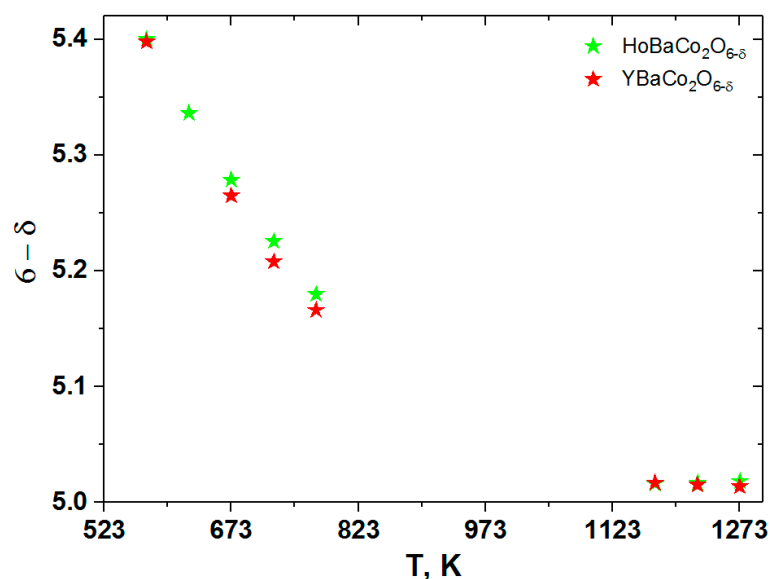


Figure 6. Oxygen content in $\text{HoBaCo}_2\text{O}_{6-\delta}$ and $\text{YBaCo}_2\text{O}_{6-\delta}$ [28] as a function of temperature in air atmosphere.

A set of nonlinear equations, comprising the equilibrium constants of the defect reactions (see Table 1), the charge neutrality, and the mass balance conditions, was solved analytically with respect to the concentrations of all the defect species involved. As a result, the model equation $p\text{O}_2 = f(T, \delta, \Delta H_i^\circ, \Delta S_i^\circ)$ was obtained, where ΔH_i° , ΔS_i° are standard enthalpies and entropies of the quasi-chemical reactions, respectively (see Table 1). This equation was fitted to the combined $p\text{O}_2$ - T - δ data set. The results of fitting are summarized in Table 1 and Figure 7. As seen, the experimental values and those calculated using the model proposed coincide with each other well. It is interesting to mention that correct determination of the reaction (2) enthalpy requires the use of high-temperature data on $\text{HoBaCo}_2\text{O}_{6-\delta}$ oxygen nonstoichiometry. The reason is low concentration of nonclustered oxygen vacancies at $\delta < 1$. As a result, the data in the temperature range $T = 573$ – 773 K

can be, in principle, described using the simplified defect structure model, which does not account for the reaction (2). However, the analysis of the whole dataset requires all the defect reactions listed in the Table 1.

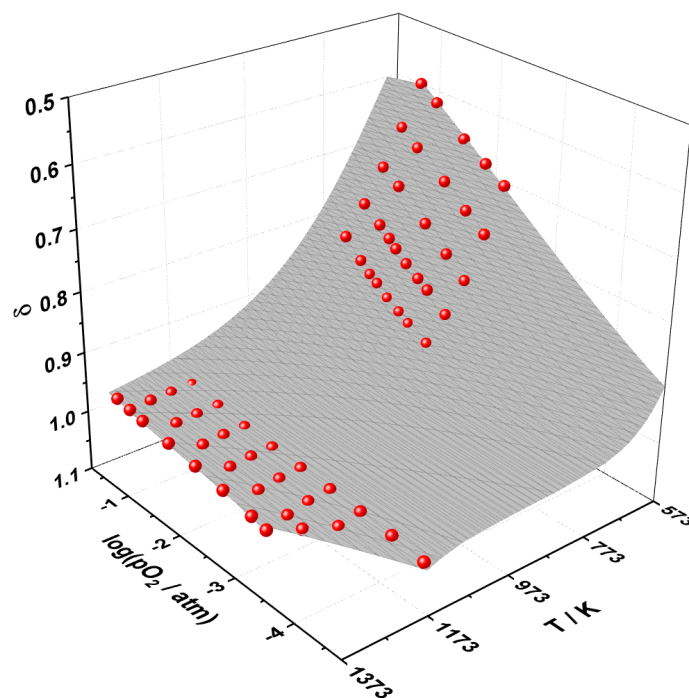


Figure 7. The results of fitting the defect structure model to the combined $p\text{O}_2$ - T - δ -dataset of $\text{HoBaCo}_2\text{O}_{6-\delta}$: the spheres correspond to the experimental values obtained in the present (573–773 K) and previous work [37] (1173–1373 K); the surface represents the model calculations.

The values of the thermodynamic functions of the defect reactions determined in the present work for HBC and those estimated earlier for other $\text{REBaCo}_2\text{O}_{6-\delta}$ [28,33–36] are given simultaneously in Figure 8 as a function of RE^{3+} -cation radius (CN = 9 radii were employed since they are available in [43] for all the RE^{3+} -cations). As seen the enthalpy of the cobalt disproportionation reaction (1) (see Table 1), being on average around $30 \text{ kJ}\cdot\text{mol}^{-1}$ is somewhat decreasing from $\text{RE} = \text{La}$ to $\text{Y}(\text{Ho})$ with decreasing RE^{3+} radius. The oxygen exchange reaction (3) (see Table 1) becomes more endothermic and the pseudo-cluster formation reaction (2), and becomes less exothermic with increasing RE^{3+} size, indicating the decreasing energy gain from oxygen vacancies preferential formation in RE^{3+} containing layers. The estimated values of the thermodynamic functions of corresponding defect reactions (1)–(3) (see Table 1) for HBC can be compared with those obtained earlier for YBC [28]. Since, as noted above, the values of the oxygen nonstoichiometry of both oxides are very close to each other, it is not surprising that enthalpies and entropies of the appropriate defect reactions (see Figure 8) are nearly equal within the uncertainty limits.

Interestingly, it seems some irregularities in the variation of thermodynamic parameters in the case of the cobaltites containing rare-earth cations possessing stable electron configurations, such as La^{3+} ([Xe]), Gd^{3+} ([Xe]4f⁷) and Y^{3+} ([Kr]), can be observed in Figure 8. The double perovskites $\text{REBaCo}_2\text{O}_{6-\delta}$ containing these three cations clearly deviate, albeit to a different extent, from the smoothed lines drawn through the points belonging to the rest of the compounds. The largest deviation is exhibited by the standard enthalpy and entropy of the quasichemical reaction (3), describing oxygen release from the oxide lattice accompanied by the formation of oxygen vacancies in the RE^{3+} -layers i.e., in the case of the oxidation reaction. Intuitively, this seems quite logical in a sense that the redox reactions are highly dependent on the electronic structure of participating chemical species especially considering that point defects as quasiparticles, being the components of the same crystal lattice, are not completely independent of each other, contrary to chemical

reagents of the real chemical reactions. However, the detailed understanding of the origin of these observations is lacking at present. As far as we know, this is the first experimental observation of the role played by the rare-earth cations in governing the redox properties of perovskites. Such data and such observations are very rare. Typically, it is believed that the 3d-metal-oxygen sublattice plays the major role in the redox properties of perovskite oxides. Although this is largely true, the influence of the rare-earth cations, as shown here, can, in some cases, be quite sensible and should not be completely ruled out. The origin of this effect should be thoroughly studied, including detailed electronic structure calculations for the $REBaCo_2O_{6-\delta}$ cobaltites.

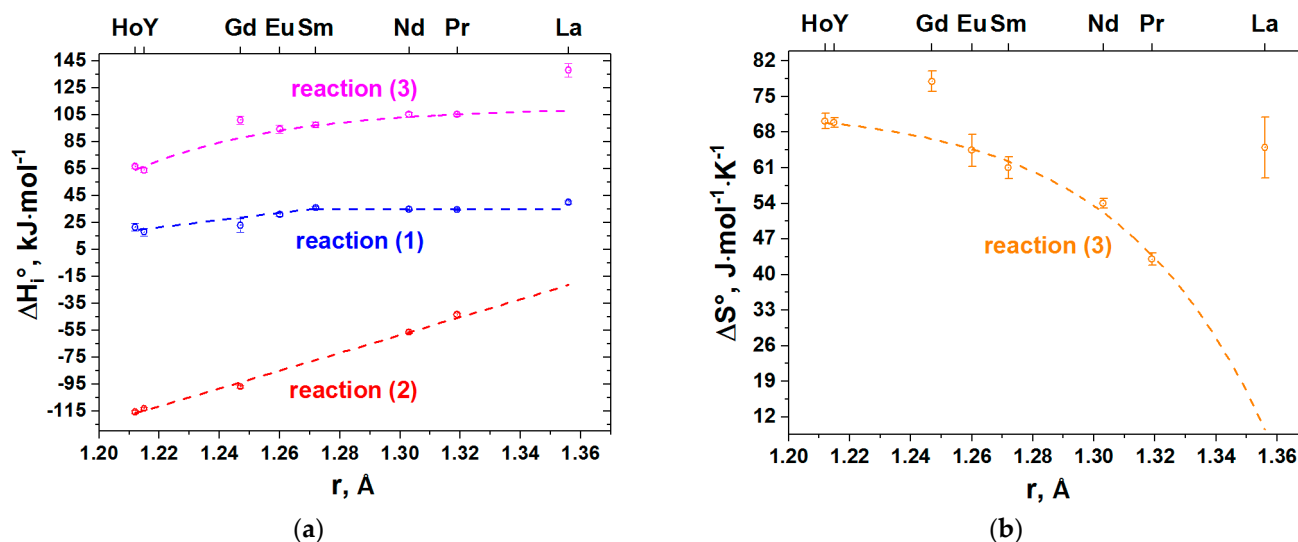


Figure 8. Dependences of ΔH_i° ($i = 1-3$) (a) and ΔS_3° (b) on RE^{3+} radius (crystal radii of 9-coordinated RE^{3+} [36]) for $REBaCo_2O_{6-\delta}$: $RE = Ho$ —the present work, $RE = La$ [33], Pr [29], Nd [34], Sm [35], Eu [35], Gd [36], and Y [28]. The lines are to guide the eye only.

4. Conclusions

The $HoBaCo_2O_{6-\delta}$ double perovskite samples were synthesized via the standard ceramic technique and were studied by DSC in the temperature range 298–773 K at different pO_2 between 0.21 and $5 \cdot 10^{-5}$ atm. DSC revealed a large endothermic effect above ca. 640 K, corresponding to oxygen release from the oxide lattice. At lower temperatures, depending on the pO_2 , which defines the actual oxygen content, $6-\delta$, in HBC, there were up to three smaller endothermic effects corresponding to phase transitions. The lower-temperature phase transition (1), exhibited by HBC samples with oxygen content spanning from 5.00 to 5.33, was identified as having magnetic origin. The endothermic effects on the DSC curves at higher temperatures were referred to the tetragonal (s.g. $P4/mmm$, 332-type superstructure) to orthorhombic (s.g. $Pmmm$ and 122-type superstructure) to tetragonal (s.g. $P4/mmm$, 112-type superstructure) phase transitions due to step by step disordering of oxygen vacancies.

The oxygen content in the single-phase tetragonal HBC was determined at $T = 573-773$ K and $pO_2 = 0.21-10^{-2.12}$ atm using TG and the flow reactor method. The data obtained in this way were used to extend the applicability range of the defect structure model proposed earlier [37] from the narrow high-temperature range of 1173–1323 K down to as low as 573 K.

The defect structure of HBC was found to be similar to that of YBC. Thermodynamic functions of defect reactions estimated for HBC were compared with those determined earlier for other $REBaCo_2O_{6-\delta}$. It was shown that the enthalpies of all the quasichemical reactions increase more or less gradually with increasing RE^{3+} cation radius in the row Ho(Y)—La whilst entropy of oxygen exchange reaction gradually decreases from Pr to Ho. The cobaltites containing rare-earth cations possessing stable electron configurations

such as La^{3+} ([Xe]), Gd^{3+} ([Xe]4f⁷) and Y^{3+} ([Kr]) deviate from these dependencies. This observation shows that the role played by the rare-earth cations in governing the redox properties and defect chemistry of perovskites is not well understood at present and needs further thorough study.

Author Contributions: Conceptualization, D.S.T.; Data curation, R.E.Y. and D.S.T.; Formal analysis, D.S.T., I.L.I., D.A.M., V.V.S. and A.Y.Z.; Funding acquisition, R.E.Y.; Investigation, R.E.Y., D.S.T., I.L.I. and D.A.M.; Methodology, D.S.T., I.L.I., D.A.M. and A.Y.Z.; Supervision, D.S.T. and A.Y.Z.; Validation, D.S.T., I.L.I., D.A.M., V.V.S. and A.Y.Z.; Writing—original draft, R.E.Y., D.S.T., I.L.I., V.V.S. and A.Y.Z.; Writing—review and editing, R.E.Y., D.S.T., V.V.S. and A.Y.Z. All authors have read and agreed to the published version of the manuscript.

Funding: The research funding from the Ministry of Science and Higher Education of the Russian Federation (Ural Federal University project within the Priority-2030 Program) is gratefully acknowledged (grant No. IIPTS48C4T28.2-23).

Data Availability Statement: The reported data are available by a reasonable request from the corresponding author.

Acknowledgments: The authors are grateful to A.L. Sednev-Lugovets for providing the original high temperature oxygen nonstoichiometry data [29] for $\text{HoBaCo}_2\text{O}_{6-\delta}$ and for fruitful discussions.

Conflicts of Interest: The authors declare no conflict of interest.

References

1. Klyndyuk, A.I.; Chizhova, E.A.; Kharytonau, D.S.; Medvedev, D.A. Layered Oxygen-Deficient Double Perovskites as Promising Cathode Materials for Solid Oxide Fuel Cells. *Materials* **2022**, *15*, 141. [CrossRef] [PubMed]
2. Rautama, E.-L.; Karppinen, M. R-site varied series of $\text{R}\text{BaCo}_2\text{O}_{5.5}$ ($\text{R}_2\text{Ba}_2\text{Co}_4\text{O}_{11}$) compounds with precisely controlled oxygen content. *J. Solid State Chem.* **2010**, *183*, 1102–1107. [CrossRef]
3. Pelosato, R.; Cordaro, G.; Stucchi, D.; Cristiani, C.; Dotelli, G. Cobalt based layered perovskites as cathode material for intermediate temperature Solid Oxide Fuel Cells: A brief review. *J. Power Source* **2015**, *298*, 46–67. [CrossRef]
4. Shen, M.; Ai, F.; Ma, H.; Xu, H.; Zhang, Y. Progress and prospects of reversible solid oxide fuel cell materials. *Iscience* **2021**, *24*, 103464. [CrossRef]
5. Joung, Y.-H.; Kang, H.-I.; Choi, W.S.; Kim, J.H. Investigation of X-Ray Photoelectron Spectroscopy and Electrical Conductivity Properties of the Layered Perovskite $\text{LnBaCo}_2\text{O}_{5+\delta}$ (Ln = Pr, Nd, Sm, and Gd) for IT-SOFC. *Electron. Mater. Lett.* **2013**, *9*, 463–465. [CrossRef]
6. Shi, Z.; Xia, T.; Meng, F.; Wang, J.; Lian, J.; Zhao, H.; Bassat, J.-M.; Grenier, J.-C.; Meng, J. A Layered Perovskite $\text{EuBaCo}_2\text{O}_{5+\delta}$ for Intermediate-Temperature Solid Oxide Fuel Cell Cathode. *Fuel Cells* **2014**, *14*, 979–990. [CrossRef]
7. Zhang, N.; Li, W.; Berry, D.; Surdoyal, W.; Shekhawat, D.; Liu, X. A New Insight into the Oxygen Reduction Reaction on High Performance Cation-Ordered PBCO Perovskite as IT-SOFC Cathode. *ECS Trans.* **2017**, *78*, 643–653. [CrossRef]
8. Zhuravleva, T.A. Electrophysical Properties of Layered Perovskites $\text{LnBaCo}_{2-x}\text{Cu}_x\text{O}_{5+\delta}$ (Ln = Sm, Nd) for Solid Oxide Fuel Cells. *Russ. J. Electrochem.* **2011**, *47*, 676–680. [CrossRef]
9. Malyshkin, D.; Novikov, A.; Ivanov, I.; Sereda, V.; Tsvetkov, D.; Zuev, A. The origin of triple conductivity and water uptake in layered double perovskites: A case study on lanthanum-substituted $\text{GdBaCo}_2\text{O}_{6-\delta}$. *J. Alloy. Compd.* **2020**, *845*, 156309. [CrossRef]
10. Kim, J.P.; Pyo, D.W.; Magnone, E.; Park, J.H. Preparation and Oxygen Permeability of $\text{ReBaCo}_2\text{O}_{5+\delta}$ (Re = Pr, Nd, Y) Ceramic Membranes. *Adv. Mater. Res.* **2012**, *560–561*, 959–964. [CrossRef]
11. Zhang, K.; Ge, L.; Ran, R.; Shao, Z.; Liu, S. Synthesis, characterization and evaluation of cation-ordered $\text{LnBaCo}_2\text{O}_{5+\delta}$ as materials of oxygen permeation membranes and cathodes of SOFCs. *Acta Mater.* **2008**, *56*, 4876–4889. [CrossRef]
12. Kundu, A.K. Magnetic perovskites. In *Engineering Materials*; Springer: Berlin/Heidelberg, Germany, 2016; 167p. [CrossRef]
13. Lafkioti, M.; Goering, E.; Gold, S.; Schütz, G.; Barilo, S.N.; Shiryaev, S.V.; Bychkov, G.L.; Lemmens, P.; Hinkov, V.; Deisenhofer, J.; et al. Spin state and orbital moments across the metal–insulator-transition of $\text{REBaCo}_2\text{O}_{5.5}$ investigated by XMCD. *New J. Phys.* **2008**, *10*, 123030. [CrossRef]
14. Zhu, M.; Guan, D.; Hu, Z.; Lin, H.-J.; Chen, C.-T.; Sheu, H.-S.; Wang, S.; Zhou, J.; Zhou, W.; Shao, Z. Synergistic effects in ordered Co oxides for boosting catalytic activity in advanced oxidation processes. *Appl. Catal. B Environ.* **2021**, *297*, 120463. [CrossRef]
15. Grimaud, A.; May, K.J.; Carlton, C.E.; Lee, Y.-L.; Risch, M.; Hong, W.T.; Zhou, J.; Shao-Horn, Y. Double perovskites as a family of highly active catalysts for oxygen evolution in alkaline solution. *Nat. Commun.* **2013**, *4*, 2439. [CrossRef]
16. Maignan, A.; Martic, C.; Pelloquin, D.; Nguyen, N.; Raveau, B. Structural and Magnetic Studies of Ordered Oxygen-Deficient Perovskites $\text{LnBaCo}_2\text{O}_{5+\delta}$, Closely Related to the “112” Structure. *J. Solid State Chem.* **1999**, *142*, 247–260. [CrossRef]
17. Chavez, E.; Mueller, M.; Moggi, L.; Caneiro, A. Study of $\text{LnBaCo}_2\text{O}_{6-\delta}$ (Ln = Pr, Nd, Sm and Gd) double perovskites as new cathode material for IT-SOFC. *J. Phys. Conf. Ser.* **2009**, *167*, 012043. [CrossRef]

18. Mejía Gómez, A.E.; Lamas, D.G.; Leyva, A.G.; Sacanell, J. Nanostructured $\text{LnBaCo}_2\text{O}_{6-\delta}$ (Ln = Sm, Gd) with layered structure for intermediate temperature solid oxide fuel cell cathodes. *AIP Adv.* **2017**, *7*, 045214. [CrossRef]
19. Gong, W.; Yadav, M.; Jacobson, A.J. A Comparison of Electrochemical Performance of Double Perovskite $\text{REBaCo}_2\text{O}_{5+x}$ Cathodes in Symmetrical Solid Oxide Fuel Cells. *MRS Online Proc. Libr.* **2008**, *1126*, 807. [CrossRef]
20. Kulka, A.; Hu, Y.; Dezanneau, G.; Molenda, J. Investigation of $\text{GdBaCo}_{2-x}\text{Fe}_x\text{O}_{5.5-\delta}$ as a cathode material for intermediate temperature solid oxide fuel cells. *Funct. Mater. Lett.* **2011**, *4*, 157–160. [CrossRef]
21. Suntsov, A.Y.; Leonidov, I.A.; Markov, A.A.; Patrakeev, M.V.; Blinovskov, Y.N.; Kozhevnikov, V.L. Oxygen Nonstoichiometry and the Thermodynamic and Structural Properties of Double Perovskites $\text{PrBaCo}_{2-x}\text{Cu}_x\text{O}_{5+\delta}$. *Russ. J. Phys. Chem. A* **2009**, *83*, 832–838. [CrossRef]
22. Yoo, S.; Shin, J.Y.; Kim, G. Thermodynamic and electrical characteristics of $\text{NdBaCo}_2\text{O}_{5+\delta}$ at various oxidation and reduction states. *J. Mater. Chem.* **2011**, *21*, 439–443. [CrossRef]
23. Wang, W.; Peh, T.S.; Chan, S.H.; Zhang, T.S. Synthesis and Characterization of $\text{LnBaCo}_2\text{O}_{5+\delta}$ Layered Perovskites as Cathodes for Intermediate-Temperature Solid Oxide Fuel Cells. *ECS Trans.* **2009**, *25*, 2277–2281. [CrossRef]
24. Bahout, M.; Pramana, S.S.; Hanlon, J.M.; Dorcet, V.; Smith, R.I.; Paofai, S.; Skinner, S.J. Stability of $\text{NdBaCo}_{2-x}\text{Mn}_x\text{O}_{5+\delta}$ ($x = 0, 0.5$) layered perovskites under humid conditions investigated by high-temperature in situ neutron powder diffraction. *J. Mater. Chem. A* **2015**, *3*, 15420–15431. [CrossRef]
25. Dong, F.; Ni, M.; Chen, Y.; Chen, D.; Tadé, M.O.; Shao, Z. Structural and oxygen-transport studies of double perovskites $\text{PrBa}_{1-x}\text{Co}_2\text{O}_{5+\delta}$ ($x = 0.00, 0.05, \text{ and } 0.10$) toward their application as superior oxygen reduction electrodes. *J. Mater. Chem. A* **2014**, *2*, 20520. [CrossRef]
26. Kim, J.-H.; Manthiram, A. $\text{LnBaCo}_2\text{O}_{5+\delta}$ oxides as cathodes for Intermediate-Temperature Solid Oxide Fuel Cells. *J. Electrochem. Soc.* **2008**, *155*, B385–B390. [CrossRef]
27. Diaz-Fernandez, Y.; Malavasi, L.; Mozzati, M.C. Effect of oxygen content on properties of the $\text{HoBaCo}_2\text{O}_{5+\delta}$ layered cobaltite. *Phys. Rev. B* **2008**, *78*, 144405. [CrossRef]
28. Yagovitin, R.E.; Tsvetkov, D.S.; Ivanov, I.L.; Malyshkin, D.A.; Sereda, V.V.; Zuev, A.Y. Thermodynamics of Formation and Disordering of $\text{YBaCo}_2\text{O}_{6-\delta}$ Double Perovskite as a Base for Novel Dense Ceramic Membrane Materials. *Membranes* **2023**, *13*, 10. [CrossRef] [PubMed]
29. Ivanov, I.L.; Zakiryanov, P.O.; Sereda, V.V.; Mazurin, M.O.; Malyshkin, D.A.; Zuev, A.Y.; Tsvetkov, D.S. Nonstoichiometry, Defect Chemistry and Oxygen Transport in Fe-Doped Layered Double Perovskite Cobaltite $\text{PrBaCo}_{2-x}\text{Fe}_x\text{O}_{6-\delta}$; ($x = 0\text{--}0.6$) Membrane Materials. *Membranes* **2022**, *12*, 1200. [CrossRef]
30. Kofstad, P. *Nonstoichiometry, Diffusion, and Electrical Conductivity in Binary Metal Oxides*; Wiley-Interscience: New York, NY, USA, 1972; p. 382.
31. Zhang, H.; Guan, D.; Gao, X.; Yu, J.; Chan, G.; Zhou, W.; Shao, Z. Morphology, crystal structure and electronic state one-step co-tuning strategy towards developing superior perovskite electrocatalyst for water oxidation. *J. Mater. Chem. A* **2019**, *7*, 19228–19233. [CrossRef]
32. Cherepanov, V.A.; Gavrilova, L.Y.; Aksenova, T.V.; Urusova, A.S.; Volkova, N.E. Synthesis, structure and properties of $\text{LnBa}(\text{Co,Me})_2\text{O}_{5+\delta}$ (Ln = Nd, Sm, Ho and Y; Me = Fe, Ni, Cu) as potential cathodes for SOFCs. *Mater. Res. Soc.* **2012**, *1384*, 7. [CrossRef]
33. Malyshkin, D.; Novikov, A.; Tsvetkov, D.; Zuev, A. Preparation, Oxygen Nonstoichiometry and Defect structure of Double Perovskite $\text{LaBaCo}_2\text{O}_{6-\delta}$. *Mater. Lett.* **2018**, *229*, 324–326. [CrossRef]
34. Tsvetkov, D.S.; Yagovitin, R.E.; Sereda, V.V.; Malyshkin, D.A.; Ivanov, I.L.; Zuev, A.Y.; Maignan, A. Defect structure and redox energetics of $\text{NdBaCo}_2\text{O}_{6-\delta}$. *Solid State Ionics* **2021**, *361*, 115549. [CrossRef]
35. Sereda, V.V.; Malyshkin, D.A.; Ivanov, I.L.; Tsvetkov, D.S.; Zuev, A.Y.; Maignan, A. Redox Thermochemistry, Thermodynamics, and Solar Energy Conversion and Storage Capability of Some Double Perovskite Cobaltites. *Inorg. Chem.* **2021**, *60*, 18141–18153. [CrossRef] [PubMed]
36. Tsvetkov, D.S.; Sednev-Lugovets, A.L.; Sereda, V.V.; Malyshkin, D.A.; Ivanov, I.L.; Zuev, A.Y. Redox energetics and enthalpy increments of $\text{GdBaCo}_2\text{O}_{6-\delta}$. *Thermochim. Acta* **2020**, *686*, 178562. [CrossRef]
37. Sednev-Lugovets, A.L. Thermodynamic Stability and Physico-Chemical Properties of Double Perovskites $\text{YBaCo}_2\text{O}_{6-\delta}$ and $\text{HoBaCo}_2\text{O}_{6-\delta}$. Ph.D. Thesis, Ural Federal University, Ekaterinburg, Russia, 2020.
38. Sednev-Lugovets, A.L.; Tsvetkov, D.S.; Sereda, V.V.; Yagovitin, R.E.; Zuev, A.Y.; Maignan, A. Defect structure and thermochemistry of $\text{YBaCo}_2\text{O}_{6-\delta}$. *Thermochim. Acta* **2021**, *698*, 178886. [CrossRef]
39. Sednev, A.L.; Tsvetkov, D.S. Study and optimization of the synthesis routine of the single phase $\text{YBaCo}_2\text{O}_{6-\delta}$ double perovskite. *Chim. Techno Acta* **2017**, *4*, 183–190. [CrossRef]
40. Kim, J.-H.; Kim, Y.N.; Bi, Z.; Manthiram, A.; Paranthaman, M.P.; Huq, A. Overcoming phase instability of $\text{RBaCo}_2\text{O}_{5+\delta}$ (R = Y and Ho) by Sr substitution for application as cathodes in solid oxide fuel cells. *Solid State Ionics* **2013**, *253*, 81–87. [CrossRef]
41. Rietica. Available online: <http://rietica.org/> (accessed on 24 August 2023).
42. Zuev, A.Y.; Tsvetkov, D.S. Conventional methods for measurements of chemo-mechanical coupling. In *Electro-Chemo-Mechanics of Solids*; Bishop, S.R., Perry, N., Marrocchelli, D., Sheldon, B., Eds.; Springer International Publishing: Berlin, Germany, 2017; pp. 5–35.

43. Shannon, R.D. Revised Effective Ionic Radii and Systematic Studies of Interatomic Distances in Halides and Chalcogenides. *Acta Cryst.* **1976**, *32*, 751. [[CrossRef](#)]
44. Suard, E.; Fauth, F.; Caignaert, V.; Mirebeau, I.; Baldinozzi, G. Charge ordering in the layered Co-based perovskite HoBaCo₂O₅. *Phys. Rev. B* **2000**, *61*, R11871(R). [[CrossRef](#)]
45. Fauth, F.; Suard, E.; Caignaert, V.; Domengès, B.; Mirebeau, I.; Keller, L. Interplay of structural, magnetic and transport properties in the layered Co-based perovskite LnBaCo₂O₅ (Ln = Tb, Dy, Ho). *Eur. Phys. J. B* **2001**, *21*, 163–174. [[CrossRef](#)]

Disclaimer/Publisher's Note: The statements, opinions and data contained in all publications are solely those of the individual author(s) and contributor(s) and not of MDPI and/or the editor(s). MDPI and/or the editor(s) disclaim responsibility for any injury to people or property resulting from any ideas, methods, instructions or products referred to in the content.